# THE MANY FACES OF FOPI FROM FRAGMENT TO STRANGENESS DETECTOR*

B. Sikora

FOPI Collaboration

Institute of Experimental Physics, Warsaw University
Hoża 69, 00-681 Warsaw, Poland

*(Received January 4, 2000)*

The FOPI detector system has been built to study the properties of dense and hot nuclear matter with the beam (0.1–2 GeV/nucleon) of the heavy ion synchrotron SIS at GSI Darmstadt. A modular system covering nearly the full $4\pi$ solid angle has been assembled in stages between 1990 and 1995, having already been used since 1991 in various experiments employing its expanding capabilities. Since the first phase of experiments, when nucleons and intermediate mass fragments could be detected at projectile- and midrapidity, FOPI developed into a specialized system detecting also pions, kaons, antikaons and identifying signals from decays of neutral particles with a strange quark content like $\Lambda$, $\Phi$ and $K^0_S$. Studies of strangeness production and propagation became an important new line of the FOPI research programme. In order to extend the strangeness research and include kaon studies in heaviest systems an upgrade program for the FOPI detector system has been started. It aims at broadening the phase space of $K^+$ and $K^-$ identification and at extending the efficiency as well as selectivity of data collecting. The upgrade of the subdetectors mainly involves the modification of TOF detectors by replacing a part of the scintillator layer with Pestov spark counters. New experiments are expected to begin in 2001. The capabilities of the FOPI system are illustrated by examples of recent and earlier results.

PACS numbers: 29.90.+r, 25.75.–q

## 1. Introduction

The $4\pi$ FOPI detector system has been built [1,2] to study collisions of heavy nuclei using the beams (0.1–2 A GeV) of the Heavy Ion Synchrotron

* Invited talk presented at the NATO Advanced Research Workshop, Krzyże, Poland 2–4 September 1999.

at GSI Darmstadt. The available beams allow to investigate a variety of phenomena reflecting the underlying reaction mechanism, from mean-field effects domination at lower energies to the excitation of internal nucleonic degrees of freedom in $N$–$N$ interactions at highest energies. Information on the collision scenario is carried by reaction products including nucleons, clusters of nucleons, mesons and hyperons. In order to obtain the most complete event characterization possible, with emphasis laid on central collisions of heavy nuclei, the following features were adopted as guide lines in the design of FOPI:

- large acceptance — nearly $4\pi$ in the c.m. systems,
- high granularity, sufficient to cope with the expected high product multiplicities,
- good particle identification in the mass- and charge range from pions to intermediate mass fragments of $A \approx 20$,
- large dynamic range with low detection thresholds.

Since these conditions translate into different sets of detector parameters depending on the laboratory polar angle and the type of particle, a modular design was adopted as compromise, with subdetectors and combinations of them optimized for the registration of reaction products of particular types. The modular design allowed to subdivide the construction of the FOPI detector system into stages and permitted in addition the start of an experimental program with the first completed detector subsystem (the so called Forward Wall) from the beginning of the SIS operation in 1991.

The present full configuration of FOPI reached substantially in 1995 is described here with emphasis on the particle identification techniques. Detailed physical parameters of the detectors as well as a description of the data aquisition system, triggers and calibration methods can be found in references [1] and [2]. The capabilities of the FOPI facility are in the following illustrated by examples of physical results.

## 2. The full configuration of FOPI

The present configuration of FOPI is shown in Fig. 1. Almost full azimuthal coverage is obtained by using detectors of nearly circular geometry. The deviation from circular symmetry is largest in the case of Outer Wall and Parabola. They consist of 8 sectors covering regular octogons centered at the beam axis.

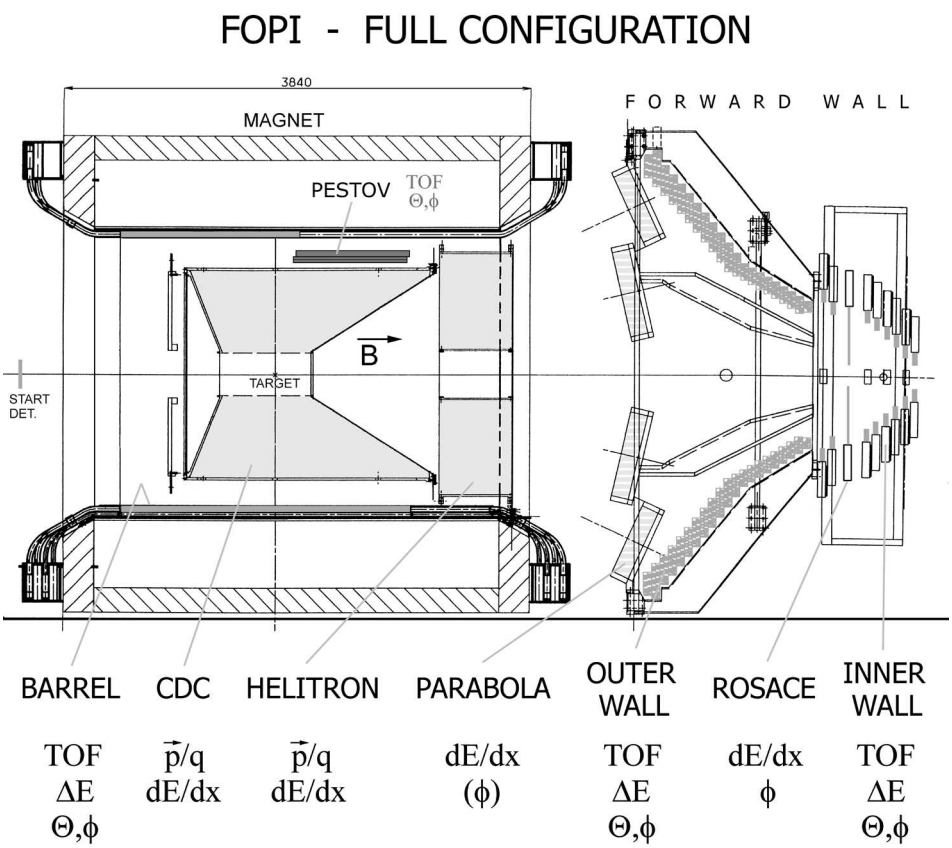


Fig. 1. Full configuration of FOPI. A vertical section along the beam axis is shown of the azimuthally nearly symmetric system. Main types of detectors are differentiated by shading: gas-filled tracking chambers — light gray, ionization chamber — stripped light gray, plastic scintillators — medium gray. The measured quantities are indicated for each detector subsystem. Parabola, Outer Wall, Rosace and Inner Wall form a system called Forward Wall. The Helitron installed in 1995/96 principally as a tracking device, has also overtaken from Parabola the role of $dE/dx$ detector in front of the Outer Wall. The upper part of section (with Pestov counters) presents the planned future configuration, a result of the upgrade project described in the last section of the text.

Two main types of detectors are used throughout the FOPI system presently. They are:

- multiwire proportional chambers placed in magnetic field, used for track reconstruction based on drift times and yielding also $dE/dx$ information — CDC (Central Drift Chamber) and Helitron,

- plastic scintillation detectors, providing at least one of the parameters: deposited energy, time of flight (TOF) and coordinates of the hit position (as listed in Fig. 1) — Barrel, Outer Wall, Inner Wall and Rosace.

In the first phase of experiments at lower energies (up to 800 $A$ MeV) a shell of ionization chambers , the so called Parabola was used. Its task, to support the identification of fragments by $dE/dx$ information, is presently taken up by the Helitron.

The hit position in the 512 scintillator strips forming the Outer Wall and in the 180 Barrel strips is derived from the times of pulses from two photomultipliers coupled to the ends of each strip [1]. The localization of hits in other scintillation detectors is possible due to their granularity: 252 compact scintillators of the Inner Wall and 60 radially arranged paddles of the Rosace, both covering the polar angle range $1.2^\circ < \Theta_{\rm lab} < 7^\circ$.

## 3. FOPI as fragment detector

Charged particles between $Z = 1$ and $Z = 15$ were detected in a number of experiments. Au + Au collisions were studied in the first series of experiments at beam energies between 100 and 800A MeV with the Forward Wall covering the range $1.2^\circ < \Theta_{\rm lab} < 30^\circ$. The $Z$ resolution obtained with the use of energy loss and TOF information, both provided by Outer Wall, is illustrated by the spectrum in Fig. 2. By combining the energy loss measured by Parabola and TOF by Outer Wall the charge separation could be extended to $Z \approx 20$. This also allowed to lower the detection threshold of heavier fragments so that effective thresholds ranging from 14 $A$ MeV for $Z = 1$ to 50 $A$ MeV for $Z = 15$ were reached. The $Z$ identification for smaller polar angles covered by Inner Wall and Rosace was limited to approximately $Z \leq 6$. Since the Forward Wall does not allow for mass determination, $A = 2Z$ was assumed in the data analyses for elements with $Z \geq 2$.

The angular acceptance of fragment detection was increased with the addition of the CDC tracking drift chamber [3] extending the earlier FOPI configuration. The CDC provides information on magnetic rigidity and specific energy loss of particles in the $33^\circ < \Theta_{\rm lab} < 145^\circ$ angular range and allows for mass determination (in contrast to the Forward Wall permitting $Z$ determination). The methods of identification with CDC will be described later in connection with the detection of mesons.

In experiments with registration of fragments the CDC is operated in a special mode. The mass range of identificated fragments is increased by applying a lower voltage to the inner half of anodes used to register heavier fragments (with $Z = 3$–6) requiring lower gass amplification than the energetic light particles, that reach the outer zone of CDC.

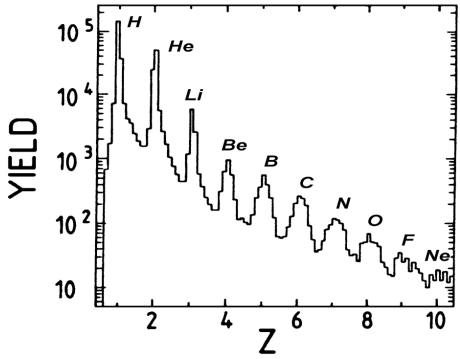


Fig. 2. Element spectrum obtained by projecting the distribution in $(v, dE/dx)$ plane onto the $Z$ parameter of the Bethe–Bloch formula. $v$ is derived from TOF measured by Outer Wall, $dE/dx$ from energy loss in Parabola.

The acceptance for light fragments of the combined Forward Wall–CDC setup is represented by an example of distribution in the normalized rapidity — transverse momentum plane shown in Fig. 3. The normalized quantities plotted are defined by $p_{\mathrm{t}}^{(0)} = (p_{\mathrm{t}}/A)/(p_{\mathrm{P}}^{\mathrm{cm}}/A_{\mathrm{P}})$ and $y^{(0)} = (y/y_{\mathrm{P}})^{\mathrm{cm}}$, where the subscript P denotes the projectile.

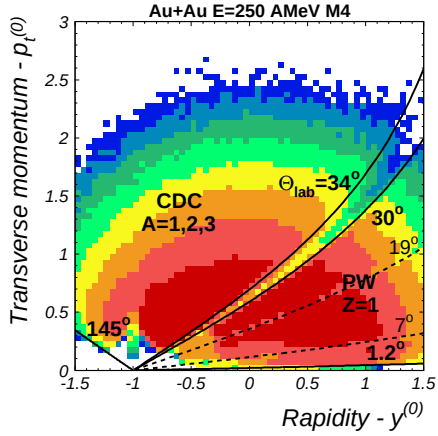


Fig. 3. FOPI acceptance. The limiting polar angles are indicated for the subdetectors: Inner Wall (1.2°,7°), Outer Wall (7°,30°) and CDC (34°,145°). The shadow at 19° is caused by the inner frame of Parabola. The intensity distribution shown is of Hydrogene in the Forward Wall and of $A$=1,2,3 particles in the CDC emited in semicentral Au+Au reactions at 250 $A$ MeV selected by a multiplicity condition (called M4 [6]). Coordinates are defined in the text.

Taking advantage of the large acceptance and sensitivity of the FOPI detector system from protons to intermediate mass fragments the FOPI Collaboration has undertaken a program of reaction studies in the energy range 0.1–1A GeV. Symmetric $A + A$ systems were choosen with masses ranging from $A \approx 90$ (Zr) to $A$=197 (Au). The detailed study of Au + Au at 150, 250 and 400 $A$ MeV [4,5] brought the discovery of strong radial expansion, an important result, that triggered renewed activities at higher relativistic (AGS, CERN) energies [6].

The effects of radial expansion and thermal motion can be most easily demonstrated and approximately separated by making use of the mass dependence of average kinetic fragment energies shown in Fig. 4. Assuming thermal equilibrium and equal for all fragments radial distributions (profiles) of collective velocity, one can reproduce the observed linear dependence by writing

$$\langle E_{\mathrm{kin}} \rangle (A) = E_{\mathrm{thermal}} + A \times e_{\mathrm{coll}} \,, \tag{1}$$

where $e_{\mathrm{coll}}$ is the average collective energy per mass unit. The total collective (flow) and the thermal energy (hence also the temperature at freeze-out) are constrained by energy conservation.

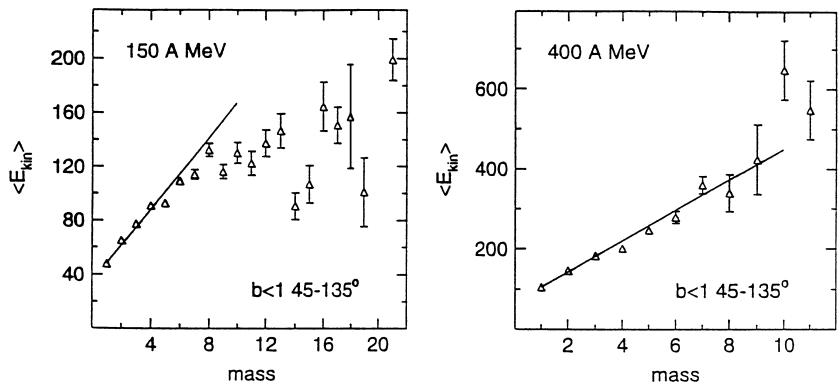


Fig. 4. Average kinetic energy as function of mass in the polar angle range 25° - 45° for Au + Au at 150 and 400 $A$ MeV. The straight lines are linear least square fits in the mass range $A$ = 1–10.

It was found that the total flow energy amounts to about 60% of the total kinetic energy. Values (0.61–0.63)±0.07 were obtained for three energies between 150 and 400 $A$ MeV [5]. Fragment energy spectra could be fitted adjusting the velocity profiles, however the results on thermal-collective energy partition are profile-independent.

## 4. Detection of charged mesons and identification via mesonic decays

The CDC and the solenoidal superconducting magnet (maximum field 0.6 T) were installed in 1992 to permit primarily measurements of charged light particles at mid- and target rapidity [3]. To extend the capability of detecting kaons, the plastic scintillator Barrrel was added as mainly a TOF detector layer in 1995.

The CDC has 16 sectors visible (as dotted lines) on the event display (Fig. 5), each containing 60 resistive wire anodes aligned parallel to the beam axis and to the magnetic field. The drift time of electrons (velocity about 40$\mu$m/ns) and the partition of charge measured at both ends of the anode are used to localize a hit, *i.e.* the position of corresponding primary ionization. Moreover the specific energy loss can be measured along the track due to proportional charge amplification. Since electrons may drift towards the anodes from two oposite directions, 2 tracks the true one and a mirror track (seen in Fig. 5), are derived from the drift times. This ambiguity is removed by inclining the plane of anodes by an angle (ca 8°) relative to the radial direction. In effect the mirror tracks can be rejected as not originating from the target. The CDC performance is characterized by the resolutions

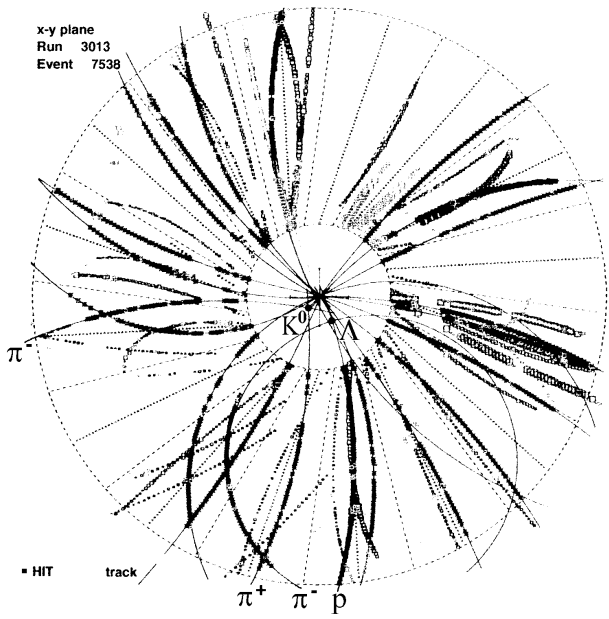


Fig. 5. Event display with CDC hits and reconstructed tracks of a $^{58}$Ni + $^{58}$Ni reaction at 1.93 $A$ GeV. For details see text.

of emission angles from the target: $\sigma_\Theta = 0.6^\circ$ in the azimuth, $\sigma_\phi = 6^\circ$ in the laboratory polar angle. The relative perpendicular momentum resolution $\sigma_{P_t}/P_t$ changes almost linearly from 4% at 0.1–0.5 MeV/$c$ to about 10% at 1.5 GeV/$c$. The $dE/dx$ measurement for $Z = 1$ particles is accurate to 5–10%. Pion identification is achieved by combining $dE/dx$ with momentum. $\pi^+$ and protons can be separated up to a limit of momentum at $p = 0.65$ GeV/$c$ caused by the intersection of their Bethe–Bloch lines. Such a limit does not exist for $\pi^-$.

The capabalities of FOPI as kaon detector are primarily a result of the simultaneous use of CDC and Barrel. The TOF detector Barrel consists of 180 strips (width×thickness×length=30×40×2400 mm$^3$) forming a cylindrical shell encircling the CDC. It covers the polar angular range $45^\circ < \Theta_{\rm lab} < 140^\circ$ and provides TOF times and hit positions. The TOF measurement can be supplemented by a velocity threshold condition supplied by a layer of water filled Cerenkov detectors (30×30×1000 mm$^3$) placed behind the scintillators at $46^\circ < \Theta_{\rm lab} < 85^\circ$. The time- and position resolutions of new installed Barrel were typically $\sigma_{\rm TOF} \approx 180$ ps and $\sigma_z \approx 3$cm. Because of aging effects in the scintillators this values were worsening (increasing ca 2 times over the years) and urging to begin the work on upgrade.

The CDC-Barrel combination provides particle velocities on curved trajectories tracked in the CDC and matched with hits in the Barrel. The methods of identification with CDC and Barrel are ilustrated in Figs. 6–9 in order of increasing selectivity by data from an Ni+Ni experiment at 1.93 $A$ GeV. $Z = 1$ particles can be separated due to the strong dependence of $dE/dx$ on particle charge. Then the masses can be determined by projecting the 2 dimensional $(dE/dx, p)$ space onto the mass parameter of the Bethe–Bloch formula. The result is shown in Fig. 6 where $dE/dx$ is plotted as function of the momentum to charge ratio $p/q$ measured by CDC. (It demonstrates also difficulties of separating heavier $Z = 1$ products.)

The measurement of TOF (and hence of velocity) with Barrel leads to a redundancy as consequence of which the particle mass can be determined by two methods. Fig. 7 shows a distribution in the momentum–velocity plane (a). Dividing the velocity by charge q allows for separate presentation of $Z = 1$ and $Z = -1$ particles. This distribution is projected onto the mass parameter in the relativistic relation $p = m\gamma\beta c$ to yield the mass distribution (b).

In order to employ the full information available, one can combine the masses derived from CDC ($C$mass) and Barrel ($B$mass).Their correlation matrix is shown in Fig. 8 for the reaction Ni+Ni at 1.93 A GeV. The best possible separation of charge 1 particles (Fig. 9) is based on the distribution of the "average" mass=($B$mass + $C$mass)/2 [7]. Several cuts were applied, the most important being the upper limit of momentum (400 MeV/$c$),

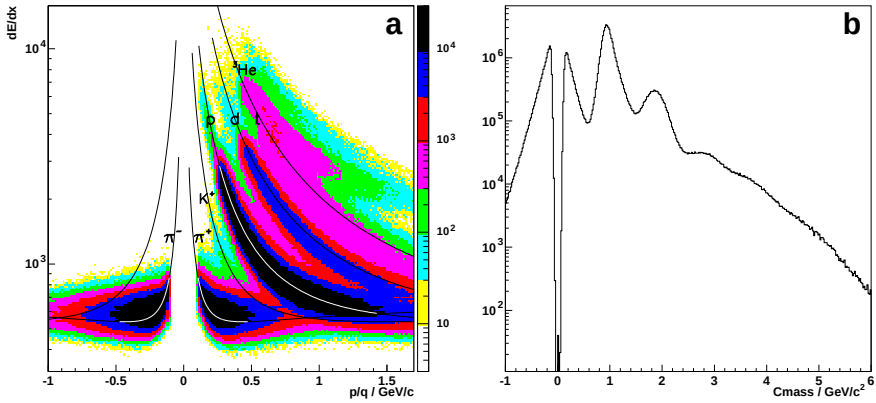


Fig. 6. Mass identification with CDC. The distribution in the $(dE/dx, p/q)$ plane (a) is projected (b) onto the mass parameter of the Bethe–Bloch formula. $C$mass denotes the mass obtained with CDC alone. Here and in Figs. 7–9 negative values on the abscissas correspond to $Z = -1$ particles.

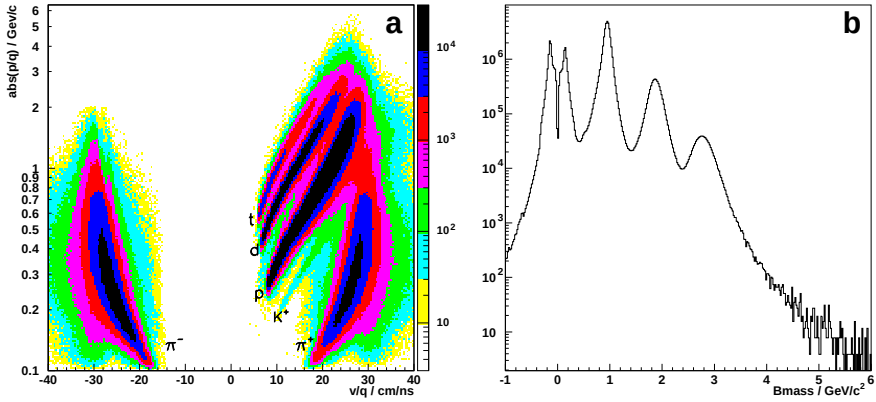


Fig. 7. Mass identification using momentum measured with CDC and time of flight measured with Barrel. For details see text.

of velocity (23 cm/ns) and of the absolute $|B\text{mass} - C\text{mass}|$ difference (150 MeV/$c^2$). The $K^+$ group (visible already in Figs. 6 and 7) and in addition the $K^-$ group can be identified at $\pm 0.5\,\text{GeV}/c^2$.

Studies of strangeness production with FOPI are not limited to kaon measurements. Meson and proton trajectories in CDC can be used to reconstruct decays of several strangeness carrying particles that decay outside the nuclear medium due to long life times. They can be identified by their

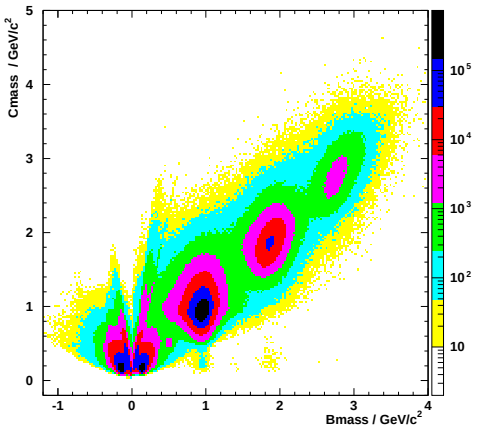


Fig. 8. Correlation matrix of masses determined by two methods. For details see text.

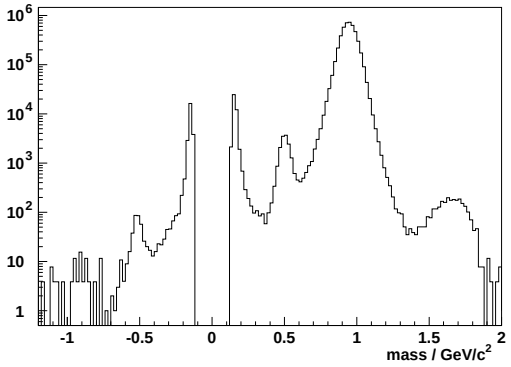


Fig. 9. Distribution of the arithmetic average of masses, *i.e.* scaled projections of the distribution in Fig. 8 onto the $C\text{mass} = |B\text{mass}|$ lines. The cuts applied are described in the text.

invariant mass. From the decays of sufficiently long living particles pairs of correlated tracks may originate from secondary vertices out of the target. The $\Lambda$ hyperon which is coproduced with kaons in elementary $N+N = K+\Lambda$ collisions decays with lifetime characterized by $c\tau = 7.9$ cm into a $\mathrm{p}\pi^-$ pair (64%). Similarily $K^0_{\mathrm{S}}$ decays with $c\tau = 2.7$ cm into a $\pi^+\pi^-$ pair (69%). A rare case of both decays within one event can be seen in Fig. 5. The invariant mass spectra are shown in Fig. 10 for the reaction Ni+Ni at 1.93 A GeV.

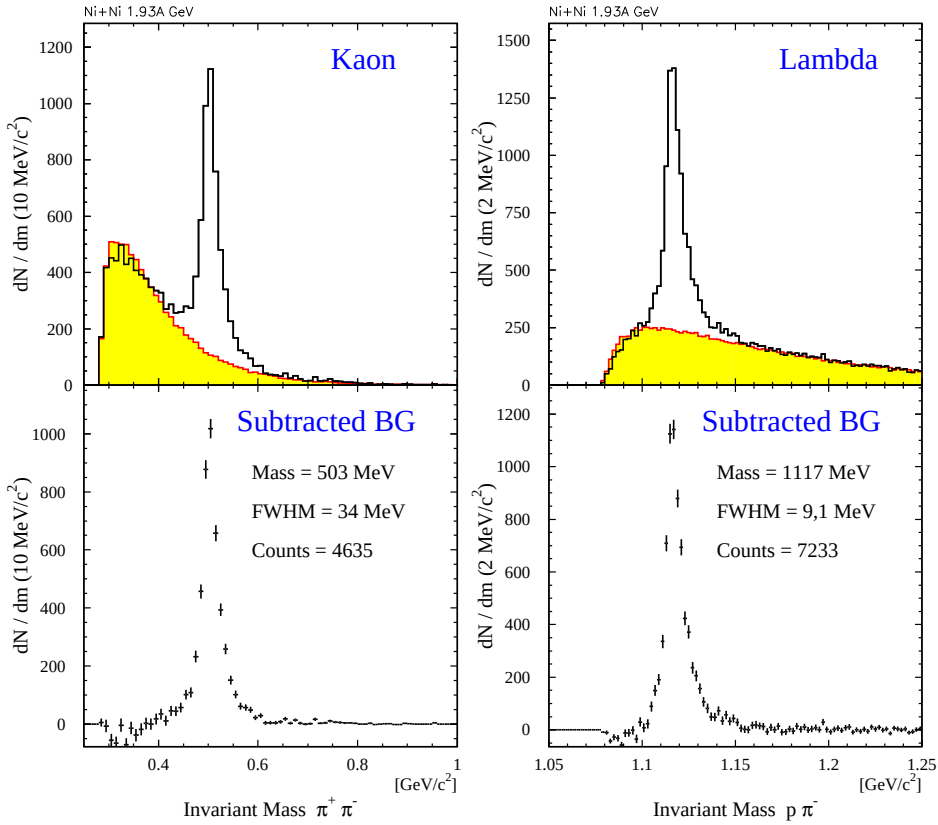


Fig. 10. Invariant mass distribution of $\pi^+\pi^-$ pairs (left panels) and $p\pi^-$ pairs (right panels) measured in the Ni + Ni experiment at 1.93 A GeV. In the lower panels combinatorial background (shaded area), simulated by mixing events, is removed. Peak positions agree within errors with masses of $K^0$ (left) and $\Lambda$ (right).

To obtain absolute intensities (in the complicated acceptance) one subtracts the bacground simulated with uncorelated trajectories from different events.

The phase space coverage of FOPI with kaon identification allows also to search for decays of the $\Phi$ meson. Free $\Phi \to K^+ + K^-$ decays are characterized by $\Gamma \approx 1.5{\cdot}10^{-22}$ s. The invariant mass spectrum measured in nucleus-nucleus reactions may therefore reflect the influence of nuclear medium on the decays that have taken place close to the surface of nuclear matter. The results obtained so far (exemplified by Fig. 11) suffer from poor statistics, but the physical effect mentioned above points to interesting options and provides guidelines for the upgrade of FOPI.

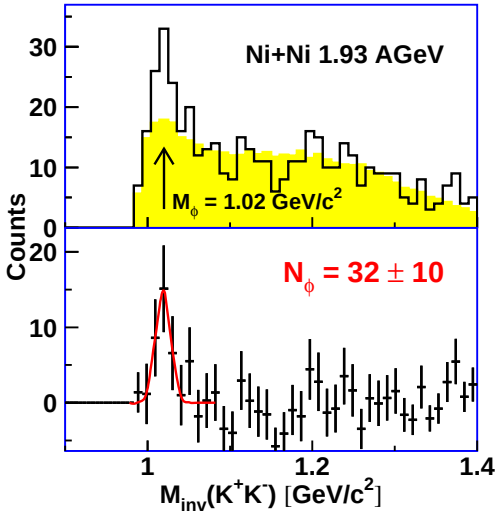


Fig. 11. The same as in Fig. 10 but for $K^+K^-$ pairs. A statistically significant peak can be related to the decay of $\Phi$ mesons.

The capabilities of FOPI have been used in a number of experiments dedicated to strangeness production and propagation. An example is shown in Fig. 12. Average in-reaction-plane transverse momenta per mass unit are plotted as function of reduced rapidity for $\Lambda$'s, kaons and protons. The upper panel demonstrates the very similar collective motion (flow) of $\Lambda$'s and protons. The behaviour of kaons is different and clearly favoures one of the kaon in-medium potentials used in the theoretical predictions [8] as shown in the lower panel. Another important result concerning the difference in dynamics of $K^+$ and $K^-$, related to their potentials, can be found in the forthcoming volume of this journal [9].

## 5. The FOPI upgrade program

Results on production and propagation of strange particles in nucleus-nucleus collisions obtained in the last years with the FOPI and KaoS detectors at GSI provided signatures that could be explained as effects of the dense hot nuclear medium. Density dependences of in medium kaon masses became a high ly debated issue as possible consequences of chiral symmetry restoration in the QCD theory (see *e.g.* [8] and references therein). In order to carry out a conclusive test of the theoretical concepts additional statistically more significant and precise measurements are necessary. The envisaged experiment measuring $K^-$ phase space distributions over a large solid angle and $\Phi$ production yields in the reaction Au+Au at 1.5 A GeV

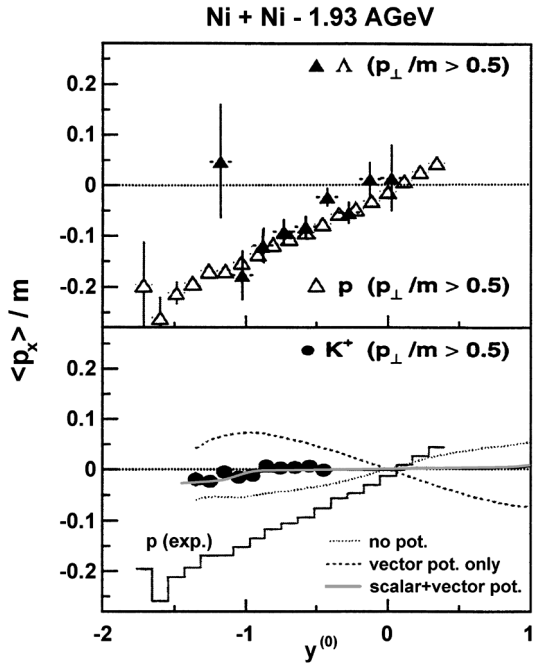


Fig. 12. Flow of protons, $\Lambda$'s and kaons in the reaction Ni + Ni at 1.93 $A$ GeV. Average in-reaction-plane transverse momenta per mass unit are plotted as function of normalized rapidity. The theoretical predictions are from Ref. [8].

(the highest SIS energy) is at present beyond the capabilities of FOPI. Such an experiment as well as many others, involving *e.g.* rare hadronic signatures, should become feasible by the FOPI upgrade program, which has been started in 1998.

The main goals are *i)* to improve the TOF measurement at $\Theta_{\rm lab}$ angles above $30^0$, both in terms of detector granularity and time resolution and *ii)* to increase the data acquisition throughput from the present 100 Hz to 800 Hz of in-beam-spill events and the tape recording speed to 10 Mb/s.

Due to multiple hits, in the mentioned Au+Au experiment the Barrel with present granularity (180 cells) would loose information on about 30% of the 50–70 charged particles emitted within its acceptance. In order to keep the multiple hit rate at tolerable level of 5–10% the granularity has to be raised by a factor of 4.

A substantial improvement of the time resolution to $\sigma_{\rm TOF}$ <100 ps would permit low background measurements of the rare $K^-$ mesons (probability $10^{-4}$ per event) and would push the upper kaon identification limit from the present 400 MeV/$c$ to approximatelly 1 GeV/$c$.

The realized program comprises the following changes of FOPI set-up:

- The scintillator strips of Barrel are being shortened to 150 cm to cover the the angles between 65° and 140°. Replacing the old extruded strips by new BC-408 material should yield resolutions better than 150 ps (as demonstrated by prototype tests), superior to the old detectors. The granularity of 180 strips is sufficient in the reduced angular range covered and remains unchanged.

- Polar angles from 68° down to 37.5° will be covered by a cylindrical shell of Pestov spark counters [10] of 90 cm length (see Fig. 1). Each of these counters has 16 individually read out strips. With each particle firing 3 to 4 strips the effective granularity exceeds 700. First 90 cm long prototypes have been developed on the basis of earlier existing 30 cm long Pestov counters and have been successfully tested [11]. A time resolution of 60 ps was reached proving that effective values better than 100 ps are a realistic goal. The spatial resolution (below 1 mm in the azimuth for the centroid of firing strips and better than 1 cm in polar direction) should substantially improve the quality of matching the tracks in CDC and the hits in the TOF shell.

The planned increased data acquisition throughput should be achieved by faster drift chamber read-out with modern scanners of the flash ADC's and by replacement of the front-end computing system with a conceptually new one. In addition an increase of data taking selectivity should result from a parallel project of designing an intelligent trigger with fast on-line track recognition.

New experiments with the upgraded FOPI detector system are expected to begin in the spring of 2001.

## REFERENCES

[1] A. Gobbi *et al.*, *Nucl. Instrum. Methods* **A324**, 156 (1993).
[2] J. Ritman, FOPI Collaboration, *Nucl. Phys. B (Proc. Suppl.)* **B44**, 708 (1995).
[3] D. Pelte *et al.*, *Z. Phys.* **A357**, 215(1997).
[4] W. Reisdorf, H.G. Ritter, *Annu. Rev. Nucl. Part. Sci.* **47**, 663 (1997).
[5] S.C. Jeong *et al.*, FOPI Collaboration, *Phys. Rev. Lett.* **72**, 3468 (1994).
[6] W. Reisdorf *et al.*, (FOPI Collaboration), *Nucl. Phys.* **A612**, 493 (1997).
[7] M. Kirejczyk, FOPI Collaboration, *Acta Phys. Pol.* **B29**, 401 (1997).
[8] G.Q. Ko, B.A. Li, *Phys. Rev. Lett.* **74**, 235 (1995).
[9] K. Wiśniewski (FOPI Collaboration) *Acta Phys. Pol.* **B31**, no2 (2000), in print.
[10] Yu.N. Pestov, *Nucl. Instrum. Methods* **A265**, 150 (1988).
[11] A. Devismes *et al.*, in GSI Report 99–1.